EDITORS' CHOICE

Investigation of Luminescence and Photoacoustic Properties in Ce^{3+}-Doped $Ln_3Al_5O_{12}$ (Ln = Lu, Y, Gd) Garnet

Jumpei Ueda,[a,z] Masakazu Yagi,[b] and Setsuhisa Tanabe[a]

[a]*Graduate School of Human and Environmental Studies, Kyoto University, Kyoto 606-8501, Japan*
[b]*National Institute of Technology, Kagawa College, Mitoyo-shi, Kagawa 769-1192, Japan*

Optical and photoacoustic properties of Ce^{3+}-doped lanthanide (Lu, Y, Gd) aluminum garnet were investigated. In the photoacoustic (PA) spectra, the $5d_1$ (lowest $5d$ level) band of Ce^{3+} was observed at around 450 nm in the obtained Ce^{3+}-doped garnet samples. This result shows that a part of the excited energy is converted to thermal energy, which is generated by some nonradiative processes. In $Y_3Al_5O_{12}:Ce^{3+}$, the $5d_1$ PA peak wavelength is shorter than the $5d_1$ photoluminescence excitation peak wavelength, which indicates that part of the heat generation is caused by the phonon relaxation process within $5d_1$ state. The PA intensity and luminescence quantum efficiency of the Ce^{3+}-doped gadolinium yttrium aluminum garnets ($(Gd_{0.5}Y_{0.5})_3Al_5O_{12}$, $(Gd_{0.75}Y_{0.25})_3Al_5O_{12}$) are much stronger and smaller, respectively, than those of $Y_3Al_5O_{12}:Ce^{3+}$. Based on these results and the persistent luminescence excitation spectra, we conclude that $(Gd_{0.5}Y_{0.5})_3Al_5O_{12}:Ce^{3+}$ and $(Gd_{0.75}Y_{0.25})_3Al_5O_{12}:Ce^{3+}$ possess the additional heat generation process explained by the thermal ionization.

Manuscript submitted August 18, 2016; revised manuscript received October 12, 2016. Published November 25, 2016.

Ce^{3+}-doped garnet materials have attracted a great deal of attention in w-LEDs and scintillators applications because of their intense broad absorption in a blue region, high quantum efficiency, and luminescence in various colors. These absorption and luminescence properties of the Ce^{3+} ion are derived from the $4f$-$5d$ allowed transitions. The luminescence color variation is caused by the shift of $5d$ excited level by the nephelauxetic effect (centroid shift caused by covalency) and the crystal field splitting.[1–4] The chemical formula of general garnet crystals can be expressed as $\{A\}_3[B]_2(C)_3O_{12}$, where $\{A\}$, $[B]$ and (C) represent the cations at the dodecahedral, octahedral and tetrahedral sites, respectively. The dodecahedral site to which Ce^{3+} occupies has the distorted square anti-prism structure with D_2 point-group symmetry, which results in the large crystal field splitting of $5d$ state. The split $5d$ levels are referred as $5d_1$, $5d_2$, $5d_3$... from the lowest $5d$ energy level. The crystal field strength and $5d$ splitting can be changed by varying the garnet component ions. So far, the optical properties of Ce^{3+} in many garnet host compositions have been studied.[5–14]

When the dodecahedral site in $Ln_3Al_5O_{12}$ are changed from the smaller lanthanide, Ln ion to the larger Ln ion, for instance in the order of Lu, Y, Tb to Gd, the $5d_1$ energy shifts to the lower energy and quenching temperature becomes much lower.[15,16] Therefore, the luminescence quantum efficiency of Ce^{3+}:$5d_1$-$4f$ at room temperature can be decreased with increasing ionic radius of the dodecahedral site. The decrease of quantum efficiency should cause excess heat generation through some nonradiative relaxation processes.

Photoacoustic (PA) spectroscopy is one of the measurements to get information of heat generation after photon absorption. The heat flux generated by excitation light is transported in a sample and changes the surface temperature. As a result, the gas pressure in the photoacoustic chamber will be changed and the formed sound can be detected by a microphone. Grinberg et al. reported the PA spectrum of $Y_3Al_5O_{12}:Ce^{3+}$ in a wide wavelength range between 265 nm and 570 nm and discussed the results with configuration coordinate diagrams and the hot luminescence from $5d_2$ to $4f$.[17] However, the PA spectroscopy of other Ce^{3+}-doped garnet phosphors has not been reported. In this study, the PA properties of Ce^{3+}-doped multi lanthanide (Lu, Y, Gd) component aluminum garnet were investigated as a function of excitation wavelengths, and the heat generation process was discussed.

[z]E-mail: ueda.jumpei.5r@kyoto-u.ac.jp

Experimental

Polycrystalline ceramics of $Lu_3Al_5O_{12}$ (LuAG), $(Lu_{0.5}Y_{0.5})_3Al_5O_{12}$ (LuYAG), $Y_3Al_5O_{12}$ (YAG), $(Gd_{0.5}Y_{0.5})_3Al_5O_{12}$ (GdYAG), $(Gd0.75Y0.25)_3Al_5O_{12}$ (Gd75YAG) doped with Ce^{3+} (0.1% at the Ln dodecahedral site of $Ln_3Al_5O_{12}$) were synthesized by the solid-state reaction. The chemicals Lu_2O_3 (99.99%), Y_2O_3 (99.99%), Gd_2O_3 (99.99%) Al_2O_3 (99.99%) and CeO_2 (99.99%) were used as starting materials. The powders were mixed by ball milling (Fritsch, Premium Line P-7) with ethanol. The obtained slurry was dried and pulverized, and then pressed into pellets. The pellets were sintered at 1600°C for 24 h in air. The crystal phase was identified as a single phase of the garnet structure using a X-ray diffraction measurement system (Rigaku, Ultima IV). The photoluminescence (PL) and photoluminescence excitation (PLE) spectra were measured by a spectrofluorometer (RF5300, Shimadzu). Photoacoustic (PA) spectrum measurement was performed at room temperature using a microphone-installed PA cell with a SiO_2 window.[18–20] The samples were mounted into a PA cell. The sample was excited by the monochromatic light combining with a Xe lamp (Wacom, KXL500F) and a monochromator (Ritsu Oyo Kogaku, MC-20 L). The photoacoustic signal was detected by a microphone and amplified by a lock-in amplifier (NF Corporation, 5610B). For the luminescence quantum efficiency measurement, the PL spectra were measured under 438 nm LD excitation by using an integrating sphere (Labsphere, LMS-100) which was connected to a CCD (charge coupled device) spectrometer of visible range (Ocean Optics, USB2000+). A standard halogen lamp (Labsphere, SCL-600) was used for calibrating this measurement system. The luminescence quantum efficiency (QE) was estimated using an equation: QE = number of emitted photons/number of absorbed photons. The persistent luminescence excitation spectra were measured using a spectrofluorometer (RF5000, Shimadzu). The samples were charged by monochromatic light from 300 nm to 550 nm, and persistent luminescence intensity at 2 min after stopping excitation was plotted as a function of excitation wavelength.

Results and Discussion

Figure 1 shows PL and PLE spectra of $Ln_3Al_5O_{12}:Ce^{3+}$ with the different Ln composition. All the samples show the photoluminescence in the range between 450 nm and 700 nm (by the blue excitation) due to the $5d_1$-$4f$ transition of Ce^{3+}. In the PLE spectra, two PLE bands were observed at around 350 nm and 450 nm, which are attributed

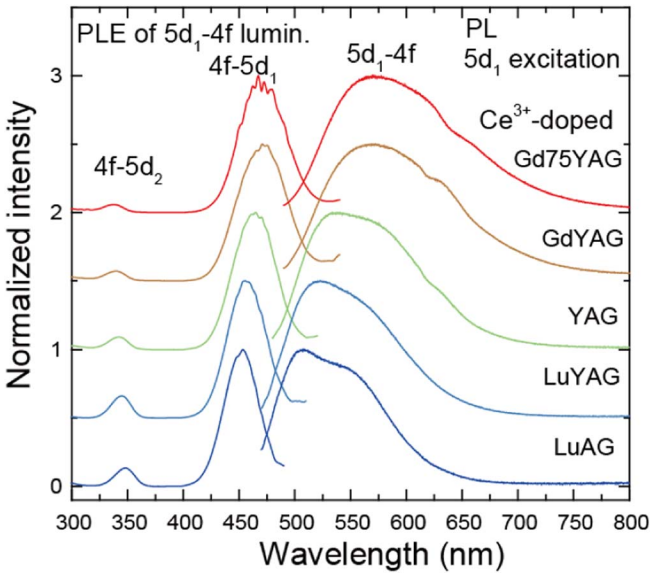

Figure 1. PL and PLE spectra of $Ln_3Al_5O_{12}:Ce^{3+}$.

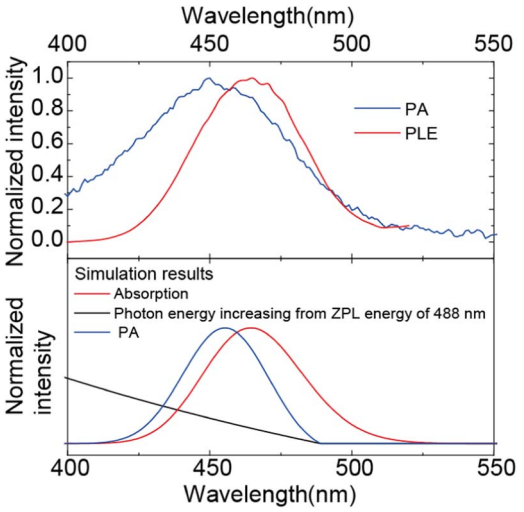

Figure 3. (a) Comparison of PLE and PA spectra in YAG:Ce^{3+}, and (b) simulation results of PA spectrum (blue solid line) estimated from the Gaussian type absorption spectra peaked at 460 nm and the change of photon energy from the ZPL energy of 488 nm.

to the 4*f*-5d_2 and 4*f*-5d_1, respectively. According to the PL and PLE, the 5d_1 energy level shifts to longer wavelength (lower energy) with increasing average ionic radius of *Ln* ion in the dodecahedral site in the order of Lu (0.977 Å), Y (1.019 Å) and Gd (1.053 Å) while the 5d_2 levels shifts to higher energy (shorter wavelength). These results are in good agreement with the previous report.[21]

Figure 2 shows photoacoustic (PA) excitation spectra of $Ln_3Al_5O_{12}:Ce^{3+}$ (*Ln* = Y, Gd, Lu) in the range between 370 nm and 600 nm. A broad PA band was observed at around 450 nm in all the samples. This PA band can be attributed to the 4*f*-5d_1 transition of Ce^{3+}. The observation of 5d_1 PA band indicates that the heat is generated after the 4*f*-5d_1 photon absorption. The intensity of 5d_1 PA band in $Ln_3Al_5O_{12}:Ce^{3+}$ becomes much stronger with increasing average ionic radius of *Ln* site. The PA intensity can be compared in the series of $Ln_3Al_5O_{12}$ because the sample sizes of the ceramics are exactly the same.

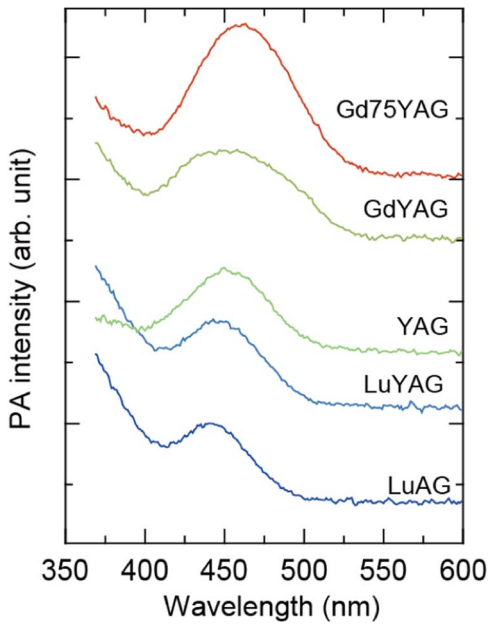

Figure 2. Photoacoustic spectra of $Ln_3Al_5O_{12}:Ce^{3+}$.

Compared with the PLE spectra, the PA peak of 5d_1 slightly shifts to shorter wavelength (higher energy) in the LuAG, LuYAG and YAG samples. Figure 3a shows the comparison between PLE and PA spectra in YAG:Ce^{3+}. The 5d_1 PA peak is located at 450 nm while the 5d_1 PLE band is at 464 nm. This mismatch of PA peak position from PLE can be explained by the wavelength dependence of the heat generation process. The heat generation can be caused by two processes. One is the nonradiative relaxation (such as thermally activated crossorver[22] and through the thermal ionization processes[23,24]) from the 5*d* state to the 4*f* ground state as shown in process 2 of Figure 4, the other is the phonon relaxation within 5d_1 state from the higher vibronic state of 5d_1 to the zero phonon state of 5d_1 as shown in the red arrow (process 1) of Figure 4. The phonon relaxation also occurs within 4*f* state (process 1′

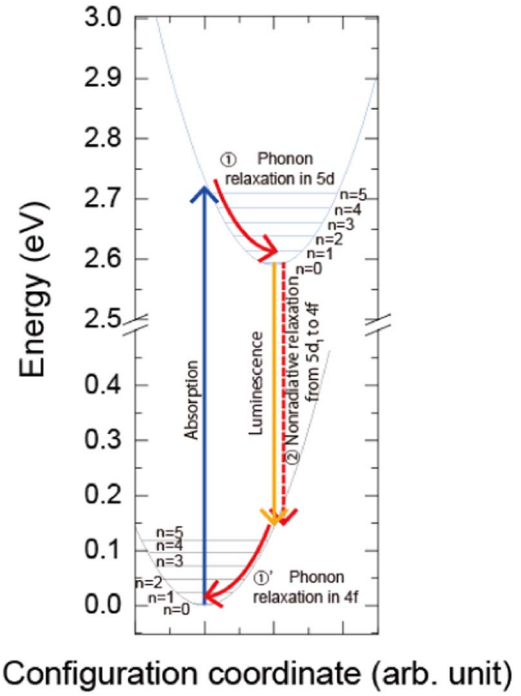

Figure 4. Schematic configuration coordinate diagram of Ce^{3+}-doped garnet.

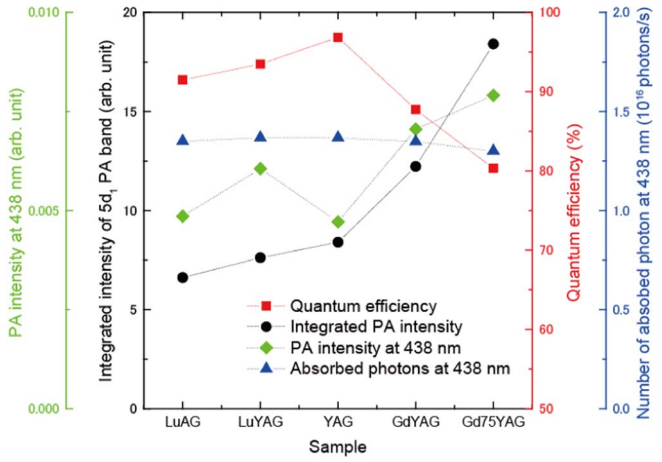

Figure 5. Integrated intensity of $5d_1$ photoacoustic band (black circle), photoacoustic intensity at 438 nm (green diamond), number of absorbed photon at 438 nm (blue triangle) and quantum efficiency by 438 nm excitation (red square) of different samples.

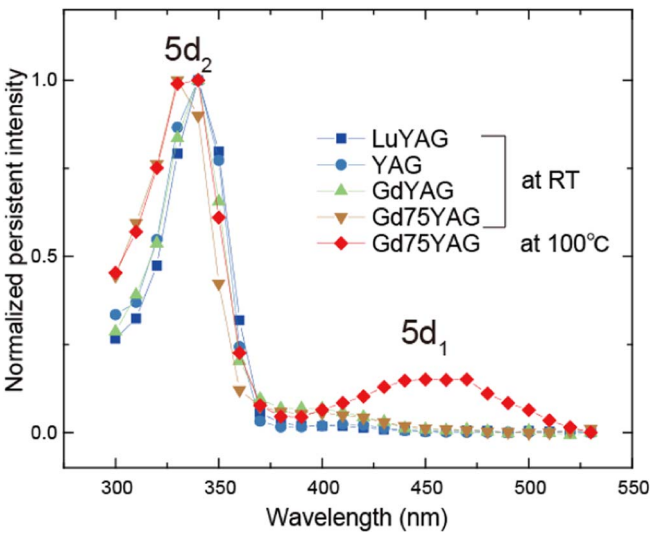

Figure 6. Persistent luminescence excitation (PersLE) spectra at room temperature in LuYAG, YAG, GdYAG and Gd75YAG doped with Ce^{3+} and PersLE spectrum at 100°C in Gd75 YAG.

of Figure 4). For the nonradiative relaxation from the $5d_1$ to the $4f$, the heat generation as a function of wavelength should be the same as the absorption spectrum. For the phonon relaxation within $5d_1$ state, the heat generation process should have the excitation wavelength dependence, which should be distinguished from the absorption spectrum. In the case of the excitation on the zero phonon line (ZPL), there is no heat generation within the $5d$ potential curve while in the excitation on higher vibronic modes in $5d$ potential curve, the heat flux is generated and increased with increasing excitation energy. Figure 3b shows a simple simulation of the wavelength dependence of heat generation by the phonon relaxation within $5d_1$ state. For the simulation, the Gaussian type absorption band (in the energy scale) peaked at 465 nm and the ZPL energy of 488 nm were assumed. The simulated absorption curve was converted to the wavelength scale as shown in red line of Figure 3b. The generating heat flux within $5d_1$ state increases with increasing excitation photon energy as the heat generation is zero at ZPL energy as shown in the black line of Figure 3b. By multiplying the generating heat flux to absorption spectra, we can roughly estimate the wavelength dependence of heat generation (PA spectrum) by the phonon relaxation within $5d_1$ state as shown in the blue line of Figure 3b. From the simulation, it is found that the peak wavelength in PA spectrum shifts to shorter wavelength compared with the absorption peak. Based on these results, the PA band of $5d_1$ in YAG:Ce^{3+} can be mainly caused by the phonon relaxation within $5d_1$ state. If the heat generation occurs by the phonon relaxation within $5d_1$ state in all the samples, the PA intensity is not different from each other because all the Ce^{3+}-doped garnet samples undergo the similar phonon relaxation within $5d_1$ state. However, with increasing average *Ln* ionic radius the integrated PA intensity increases especially from the Gd substitution as shown in Figure 5. For the integrated PA intensity, because the rising of PA intensity was observed below 450 nm, the PA spectra in the energy was fitted by Gaussian function after the exponential baseline subtraction. The increase of PA intensity with increasing *Ln* ionic radius indicates that the additional heat generation process occurs.

To understand the sample variations of PA intensity, the quantum efficiency of Ce^{3+}:$5d_1 \rightarrow 4f$ luminescence by the 438 nm LD excitation was measured. In Figure 5, the number of absorbed photons at 438 nm, quantum efficiency by 438 nm excitation, integrated PA intensity and the PA intensity at 438 nm in the different samples are shown. The quantum efficiency excited by 438 nm of LuAG:Ce, LuYAG:Ce, YAG:Ce are more than 90%, while that of GdYAG:Ce and Gd75YAG:Ce are 87% and 80%, respectively. From the QE results, the generated heat flux ratio by non-radiative process from the $5d_1$ level respect to the absorbed photons can be estimated by 100% - QE. Therefore, Gd75YAG:Ce^{3+} generates two times higher heat flux caused by nonradiative process from the $5d_1$ level compared with LuAG:Ce, LuYAG:Ce, YAG:Ce. The absorbed photon number at 438 nm is almost the same among the samples, so that the PA intensity at 438 nm can be compared. The PA intensity at 438 nm in GdYAG and Gd75YAG is much stronger compared with LuAG:Ce, LuYAG:Ce, YAG:Ce. The PA intensity at 438 nm of Gd75YAG:Ce is approximately 1.8 times higher than that of YAG:Ce. This result is corresponding to the the decrease of QE in GdYAG and Gd75YAG.

These results show that the increase of PA intensity is caused by some additional heat generation by nonradiative process. In general, two main nonradiative processes by thermally activated crossover and thermal ionization have been reported for the $5d$-$4f$ transition. Thermally activated crossover is the nonradiative relaxation process from the excited $5d$ potential curve to the lower $4f$ potential curve through the crossing point in a configuration coordinate diagram.[22] Thermal ionization is the thermally activated electron transfer process from the $5d$ state to the conduction band (CB).[23] We already demonstrated the thermal ionization quenching process in YAG:Ce^{3+} at 300°C from the thermoluminescence excitation spectroscopy.[25] The bandgap decreases with increasing lattice constant of host garnet in the order of LuAG, YAG and GdAG ($Gd_3Al_5O_{12}$), which results in the decrease of energy gap between the $5d_1$ and CB ($\Delta E_{5d\text{-}CB}$) because of the energy shift of $5d_1$ by crystal field splitting is much smaller than the that of CB.[21] The $\Delta E_{5d\text{-}CB}$ of LuAG, YAG and GdAG were estimated to be 1.05 eV, 1.07 eV and 0.6 eV, respectively.[21] Assuming that the quenching is caused by thermal ionization, it is expected that the QE at room becomes much lower and the PA intensity becomes much stronger with increasing Gd content in the garnet composition. In order to check the thermal ionization process, persistent luminescence excitation (PersLE) spectra were measured as shown in Figure 6. Persistent luminescence can be caused by detrapping of charges that were previously trapped followed by recombination on a luminescent center. Charge trapping occurs when electrons in the excited state of luminescence centers are transferred to the CB (e.g., through thermal ionization) and then captured by traps in the host. From the PersLE spectra, the threshold energy that causes the thermal ionization can be discussed. Although the obtained samples are not persistent phosphors, very weak persistent luminescence due to the Ce^{3+}:5d-4f was detected by high sensitivity photomultiplier tube. The normalized integrated intensity of persistent luminescence 2 min after ceasing excitation light was plotted as a function of excitation wavelength as shown in Figure 6. The PersLE of LuAG:Ce is not shown because the S/N ratio is very low due to the weak persistent

luminescence. In the PersLE at room temperature, the strong PersLE band was observed at around 350 nm, which can be attributed to the $4f$-$5d_2$ transition of Ce^{3+}, in all the samples. This result shows that the thermal ionization from the $5d_2$ level to the conduction band occurs at room temperature. On the other hand, in the range between 375 nm and 450 nm, only GdYAG and Gd75YAG shows weak PersLE band attributed the $5d_1$ band, which indicates that the thermal ionization from $5d_1$ level also occurs. To ensure the thermal ionization process from $5d_1$ in Gd75YAG:Ce^{3+}, the PersLE spectrum was measured at 100°C. At this temperature, the PL intensity becomes 60% respect to that at room temperature, so that the high thermal ionization probability from the $5d_1$ level can be expected. In the PersLE spectrum of Gd75YAG:Ce at 100°C, a clear excitation band was observed at around 470 nm due to the $4f$-$5d_1$ transition. This is strong evidence of thermal ionization from the $5d_1$ band. Therefore, in the Ce^{3+}-doped GdYAG and Gd75YAG, the additional heat generation can be caused by the nonradiative relaxation process from $5d_1$ to $4f$ via the thermal ionization process.

Conclusions

Ceramics of $Lu_3Al_5O_{12}$ (LuAG), $(Lu_{0.5}Y_{0.5})_3Al_5O_{12}$ (LuYAG), $Y_3Al_5O_{12}$ (YAG), $(Gd_{0.5}Y_{0.5})_3Al_5O_{12}$ (GdYAG), $(Gd0.75Y0.25)_3Al_5O_{12}$ (Gd75YAG) doped with Ce^{3+} (0.1% at the *Ln* dodecahedral site) were synthesized by solid-state reactions. By the blue excitation on the $5d_1$ state, the photoacoustic signal was detected in all the samples, which means that the excited energy is converted to the thermal energy. In YAG:Ce^{3+}, the $5d_1$ peak in the photoacoustic spectrum is 10 nm shorter than that in photoluminescence excitation spectrum. This is because the heat generation was caused by the phonon relaxation within $5d_1$ state. The PA intensity becomes much stronger with increasing average ionic radius of *Ln* site. On the other hand, the luminescence quantum efficiency becomes much lower in Ce^{3+}-doped GdYAG and Gd75YAG compared with LuAG, LuYAG and YAG. In the PersLE spectra of GdYAG and Gd75YAG, the $5d_1$ excitation band was observed, which indicated the thermal ionization occurs from the $5d_1$ level. Therefore, Ce^{3+}-doped GdYAG and Gd75YAG possess the additional heat generation process that is the nonradiative relaxation process explained by the thermal ionization.

Acknowledgment

This work was supported by JSPS KAKENHI grant Number 16K05934.

References

1. P. Dorenbos, *Phys. Rev. B*, **62**, 15640 (2000).
2. P. Dorenbos, *Phys. Rev. B*, **62**, 15650 (2000).
3. P. Dorenbos, *Phys. Rev. B*, **64**, 125117 (2001).
4. P. Dorenbos, *J. Lumin.*, **99**, 283 (2002).
5. J. W. W. Holloway and M. Kestigian, *J. Opt. Soc. Am.*, **59**, 60 (1969).
6. T. Y. Tien, E. F. Gibbons, R. G. DeLosh, P. J. Zacmanidis, D. E. Smith, and H. L. Stadler, *J. Electrochem. Soc.*, **120**, 278 (1973).
7. Y. Zorenko, T. Voznyak, V. Vistovsky, T. Zorenko, S. Nedilko, M. Batentschuk, A. Osvet, A. Winnacker, G. Zimmerer, V. Kolobanov, and D. Spassky, *Rad. Meas.*, **42**, 648 (2007).
8. M. V. Korzhik and W. P. Trower, *Appl. Phys. Lett.*, **66**, 2327 (1995).
9. J. Ueda, K. Aishima, S. Nishiura, and S. Tanabe, *Appl. Phys. Express*, **4**, 042602 (2011).
10. T. Shimizu, J. Ueda, and S. Tanabe, *Phys. Stat. Sol. c*, **9**, 2296 (2012).
11. J. Ueda, K. Aishima, and S. Tanabe, *Opt. Mater.*, **35**, 1952 (2013).
12. Z. Jiang, Y. Wang, and L. Wang, *J. Electrochem. Soc.*, **157**, J155 (2010).
13. A. A. Setlur, W. J. Heward, Y. Gao, A. M. Srivastava, R. G. Chandran, and M. V. Shankar, *Chem. Mater.*, **18**, 3314 (2006).
14. J. L. Wu, G. Gundiah, and A. K. Cheetham, *Chem. Phys. Lett.*, **441**, 250 (2007).
15. H. Shi, C. Zhu, J. Huang, J. Chen, D. Chen, W. Wang, F. Wang, Y. Cao, and X. Yuan, *Optical Materials Express*, **4**, 649 (2014).
16. C. C. Chiang, M. S. Tsai, and M. H. Hon, *J. Electrochem. Soc.*, **155**, 517 (2008).
17. M. Grinberg, A. Sikorska, and S. Kaczmarek, *J. Alloys Compd.*, **300**, 158 (2000).
18. M. Yagi and T. Morimune, Japan Pat. 5388306 (2013).
19. T. Terasako, T. Murakami, M. Yagi, and S. Shirakata, *Thin Solid Films*, **549**, 292 (2013).
20. A. Atarashi, M. Yagi, and S. Shirakata, *Jpn. J. Appl. Phys.*, **53**, 05FW12 (2014).
21. P. Dorenbos, *J. Lumin.*, **134**, 310 (2013).
22. C. Struck and W. Fonger, *Understanding Luminescence Spectra and Efficiency Using W p and Related Functions*, Springer Berlin Heidelberg, Berlin, Germany (1991).
23. W. M. Yen, M. Raukas, S. A. Basun, W. van Schaik, and U. Happek, *J. Lumin.*, **69**, 287 (1996).
24. J. Ueda, S. Tanabe, and T. Nakanishi, *J. Appl. Phys.*, **110**, 053102 (2011).
25. J. Ueda, P. Dorenbos, A. J. J. Bos, A. Meijerink, and S. Tanabe, *J. Phys. Chem. C*, **119**, 25003 (2015).